

Photoluminescence study of excitons localized in indirect-gap $\text{GaAs}_{1-x}\text{P}_x$

Shui T. Lai

Materials Research Laboratory, Allied Corporation, Morristown, New Jersey 07960

M. V. Klein

Department of Physics and Materials Research Laboratory, University of Illinois at Urbana—Champaign, Urbana, Illinois 61801

(Received 6 October 1983)

A novel structure (M_0^X) in the photoluminescence spectra from n -type indirect-gap $\text{GaAs}_{1-x}\text{P}_x$ alloys has been studied in detail. It has an asymmetric line shape and prominent X -point phonon sidebands. Its binding energy relative to the free-exciton band edge (E_{gx}^X) is very shallow. The characteristic lifetime of fluorescence decay has been found to vary rapidly over the M_0^X band linewidth. It is proposed that the M_0^X band is due to exciton bound by potential wells resulting from the alloy compositional fluctuation. The narrowing of the M_0^X band's linewidth at rising temperatures and the temperature quenching of fluorescence with the excited state can be accounted for by the strong energy dependence of the effective range of the localized exciton wave function. The decrease of the M_0^X quantum efficiency with increasing laser power is attributed to Auger decay of biexcitons.

I. INTRODUCTION

In semiconducting solid solutions many of the optical properties may be understood by applying band-structure concepts appropriate for crystals with translational symmetry.¹ Random compositional disorder is then treated as a perturbation which caused nonlinear dependence of band energies on the composition² and smears the band edges,^{3,4} as observed in absorption measurements.^{5,6} In alloys that have an indirect-gap average band structure the disorder breaks the wave-vector selection rule that forbids zero-phonon optical absorption.⁶ The resulting absorption and the related zero-phonon emission intensity are weak. The work on disorder induced by doping has been reviewed by Efros.⁷

Theoretical work on band-edge smearing may be extended to Mott-Wannier excitons in the presence of compositional disorder.⁴ States sufficiently deep in the tail of the band are thought to be localized in the sense that the wave functions have limited range.^{8,9} This does not mean that localized excitons do not "move." Even at low temperatures it is possible for them to tunnel nonelastically to lower energy states that are spatially accessible.

There have been two observations of photoluminescence (PL) features in indirect-gap semiconductor alloys that may be interpreted as a recombination of Mott-Wannier excitons that remain in localized states before they decay. The present authors reported a new PL band, M_0^X , in lightly doped n -type indirect-gap $\text{GaAs}_{1-x}\text{P}_x$ alloys.¹⁰ This band was positioned about halfway between the "free-exciton" band E_{gx}^X and D_0^X , the band due to excitons bound to neutral donors. M_0^X appeared only at the lowest temperatures and at very low excitation power densities. Decays following pulsed excitation were reported in Ref. 10 to be nonexponential with characteristic times far longer than the lifetime of D_0^X . A tentative assignment of M_0^X was made to be the recombination of localized exci-

tons (in the above sense). The present paper will present more data on M_0^X and discuss them qualitatively with the use of this localization hypothesis.

Since our report of the M_0^X exciton, observation of a similarly localized exciton has been reported in the indirect-gap $\text{Ga}_{1-x}\text{Al}_x\text{As}$ system.¹¹ A satisfactory fit to the nonexponential decay characteristics for nearly direct alloys has also been worked out based on a distribution of radiative lifetime.¹² In the $\text{GaAs}_{1-x}\text{P}_x$ work performed so far, radiative lifetimes were so long that nonradiative decays tend to dominate. The quenching center is short lived, and the nonexponential decay is governed by the tunneling probability to this essentially nonradiative exciton trap. This requires that the average exciton lifetime is to be determined by its binding energy. The very sensitive dependence of its wave function on its binding energy can be inferred from our data.

II. EXPERIMENTAL

Samples were purchased from Monsanto Corporation. They were grown by vapor phase epitaxy on [100] GaP substrates and doped with Te, Se, or S in the range of $(4-10) \times 10^{16} \text{ cm}^{-3}$. High sample quality was necessary for the observation of M_0^X centers. Samples were mounted on a copper plate and cooled in a Janis "Vari-temp" cryostat. PL was excited above the band gap with 5145-, 4880-, or 4579-Å lines from an argon laser and in the band-gap region with a cw dye laser. Front surface excitation was used, and the emitted radiation was collected and focused at 3:1 magnification onto the entrance slit of a Spex model 1400 $\frac{3}{4}$ -m double monochromator. The detector was an RCA C31034 photomultiplier tube. The input power on the sample was varied by neutral density filters.

The effect of varying the penetration depth of the exciting light on the PL spectrum was studied by using the ul-

traviolet lines from the argon laser at 3511 and 3538 Å and also yellow light from a dye laser just above the band gap of the alloy. There was practically no change in the overall line shape. The same shape was observed from samples with no GaP substrate. We observed some strain effects from the substrate on the epitaxial layer: The PL from the rectangular samples was found to be partially polarized, but the shape of the spectrum was hardly affected.

For time-dependent data the laser beam was chopped using an acousto-optic modulator. The time-delayed spectra were taken using a gated photon-counting system. The time dependence of fluorescence at fixed wavelength was recorded using a multichannel analyzer.

III. RESULTS

A. Phonon sidebands

In Fig. 1 the PL spectra of M_0^X are shown along with its LA(X) and TO(X) phonon sidebands together with the donor-bound exciton line, D_0^X . Similar data were shown in Fig. 1 of Ref. 10 using a different exciting wavelength. In a $x=0.86$ sample the new PL band labeled M_0^X is observed at 5503 Å. It is found at 12.7 meV above D_0^X . The full width at half maximum (FWHM) of the M_0^X band remains almost constant for different x and is about 3.5

meV, compared with a FWHM of 10 meV for the D_0^X band at $x=0.86$. Two other prominent features in the PL spectra are labeled LA_M^X and TO_M^X . The intensity of these two bands changes similar to that of M_0^X with increasing temperature, indicating that they are phonon sidebands of M_0^X . A study of the donor-bound excitons in the alloys¹³ showed that the longitudinal-acoustic phonon (LA) and the transverse-optical (TO) phonon sidebands from the neutral-donor-exciton PL are broadened by the alloy fluctuation in a way similar to their parent peak D_0^X . These phonon sidebands from D_0^X remain discernible in all indirect-gap alloys and are denoted LA_D^X and TO_D^X , respectively. The peaks LA_M^X and TO_M^X have the same splittings from M_0^X as LA_D^X and TO_D^X phonon sidebands from D_0^X . We assign them to be the LA- and TO-phonon assisted M_0^X exciton recombination at the X-point zone boundary. The two lower curves in Fig. 1 give similar results for $x=0.66$ and 0.50.

The TA(X) sideband of M_0^X is masked by the D_0^X PL peak in Fig. 1. Since D_0^X has a shorter lifetime than M_0^X and its sidebands,¹⁰ it is possible to remove the former from the latter by time-delayed PL. The result is shown for the $x=0.50$ sample in Fig. 3. The spectra of M_0^X and its sidebands allow an accurate determination of the phonon energies. The results are shown in Table I where they are compared with neutron data on GaP,¹⁴ piezo-transmission measurements on GaAs_{1-x}P_x (Ref. 15), and neutron measurements on GaAs.¹⁶ The tabulated results for phonon energies in GaP were obtained from a spectrum of D_0^X and its sidebands under resonant laser excitation at 2.2 K. The various entries in Table I are generally consistent, considering differences in temperature and resolution.

Genzel and Bauhofer have discussed phonon features in several alloys using a simple no-crossing model.¹⁷ We apply this picture to our results. Note that the observed energies of TA(X) and LA(X) monotonically decrease as x decreases, whereas the TO(X) energy increases. The TO(X) and LO(X) modes in the alloy merge into a phosphorous local mode in GaAs as $x \rightarrow 0$.⁶ The LA(X) mode of GaP is predicted to interact with the As gap mode of GaP and shows relatively little dependence of its frequen-

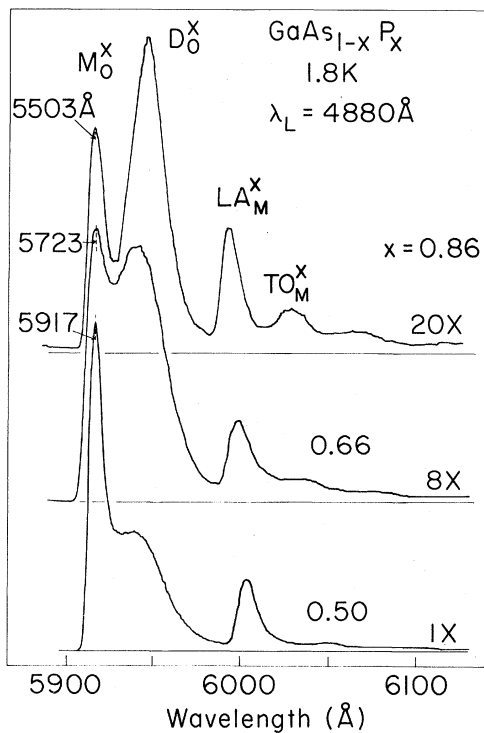


FIG. 1. PL spectra for three alloy compositions as a function of wavelength. The zero-phonon PL of the localized exciton and its LA and TO phonon sidebands are labeled M_0^X , LA_M^X , and TO_M^X , respectively. The broad peak D_0^X is due to excitons bound to neutral donors. The spectra for $x=0.86$ and 0.66 have been shifted so that the three M_0^X peaks line up. Data on the three samples were taken with same geometry, laser power, image size, and temperature.

TABLE I. Phonon energies (meV) for GaAs_{1-x}P_x.

	TA(X)	LA(X)	TO(X)	LO(X)
GaP ^a	13.2	30.9	43.8	45.4
GaP ^b	13	32		
GaP ^c	13.2	31.5	45.9	
$x=0.86^c$	12.8	31.2	45.6	
0.85 ^b	13	32		46
0.75 ^b	13	32		45
0.66 ^c	12.4	30.7	46.2	
0.59 ^b		29–32		
0.50 ^c	11.0	30.8	46.2	
GaAs ^d	9.8	28.1	31.3	29.9

^aReference 14 (300 K).

^bReference 15 (10–300 K).

^cThis work (2–3 K).

^dReference 16 (296 K).

cy on x . Table I shows this to be the case. The large predicted x dependence of the frequency of TA(X) is not observed, but this prediction was less concrete than those involving LA(X) and TO(X).¹⁷

The shallow binding energy of M_0^X and its coupling to the X-point phonons suggest that the M_0^X exciton is effective-mass-like and associated with the X-point conduction-band edge. This characteristic eliminates the possibility that M_0^X may be associated with isoelectronic traps. In the case of an isoelectronic trap, for example, the electron feels a very short-range potential of the Slater-Koster type.¹⁸ Its wave function is derived from the conduction band as a whole, and it couples to phonons throughout the Brillouin zone.

B. Temperature dependence

The peak intensity of M_0^X decreases rapidly with a relatively small increase in temperature. This was shown in Fig. 3 of Ref. 10 for the $x=0.50$ sample and is shown here in Fig. 2 for the $x=0.86$ sample. By 5.5 K M_0^X is merely a shoulder on D_0^X , and it is essentially gone by 8.2 K. At the latter temperature the weak LA_D^X donor sideband is visible, now no longer masked by the stronger LA_M^X sideband.

An important feature of the M_0^X band is its shift to lower energy while it loses intensity with increasing temperature. This is readily apparent from the top four curves in Fig. 2. This shift also applies to its phonon sideband. This effect is not due to a temperature dependence of the band gap; the D_0^X peak does not move in this temperature interval.

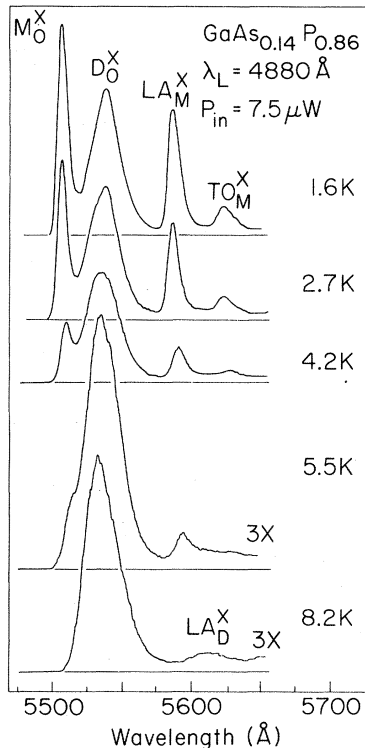


FIG. 2. Temperature-dependent PL for $x=0.86$. Labeling as in Fig. 1. LA_D^X denotes the LA-phonon sideband of D_0^X .

The shift in peak energy is also quite pronounced in the temperature-dependent, time-delayed spectra shown in Fig. 3 for the $x=0.50$ sample. The 4 μ s delay is sufficient for D_0^X to have completely decayed. Note also that the M_0^X line becomes slightly narrower with increasing temperature. The M_0^X intensity drops by factors of 4 and 50 as the temperature is raised from 2.6 to 4.9 and 6.5 K, respectively. The broad feature near 5960 Å in the lowest curve has not been studied in detail. We speculate that it originates from the phonon-assisted energy-transfer process among the localized excitons to the lower-energy bound states.

Our explanation for these temperature-dependent features of M_0^X depends on the assumption of a distribution of the nonradiative decay rate W_{nr} due to phonon-assisted tunneling. Let W_0 and W_1 denote the no-phonon and one-phonon radiative decay rates. The quantum efficiency for the no-phonon line is

$$\eta_0 = \left\langle \frac{W_0}{W_0 + W_1 + W_{nr}} \right\rangle. \quad (1)$$

The average in Eq. (1) is over the distributions of W_0 and W_{nr} . W_0 and W_1 are the zero-phonon and one-phonon decay rates, respectively, and are assumed to be essentially independent of the exciton binding energy. Details of the finer energy dependence of W_0 and W_1 have also been observed and are described in Sec. IIID. We assume that W_{nr} is due to phonon-assisted tunneling to deeper centers such as D_0^X . If the distance between the centers is r , then

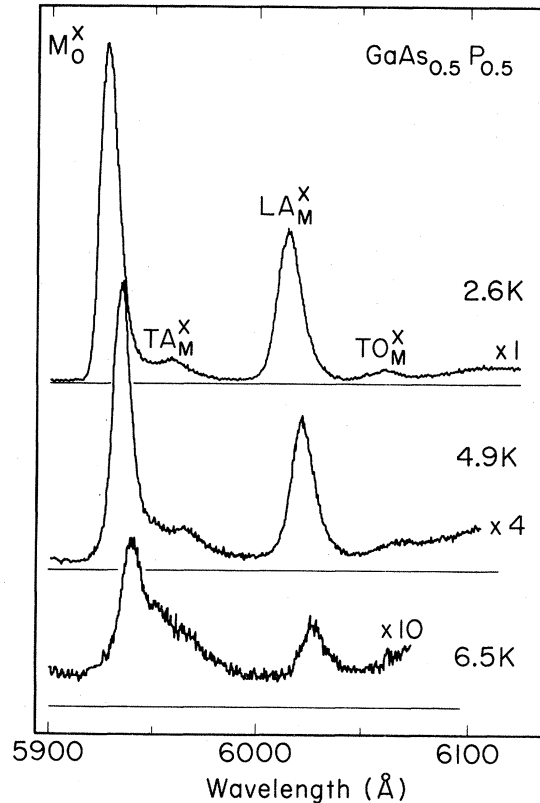


FIG. 3. Time-delayed spectra of M_0^X and its phonon sidebands at various temperatures for $x=0.5$. The spectra were taken with a 1- μ s gate 4 μ s after laser shutoff. Note the narrowing and shift of M_0^X to lower energy with rising temperature.

W_{nr} takes the following form within a model that neglects the electron-valley degeneracy:

$$W_{nr} = W_0 e^{-2\alpha r}, \quad (2a)$$

where

$$2\alpha = \hbar^{-1} (2m^* E_b)^{1/2}, \quad (2b)$$

with m^* equal to exciton effective mass and E_b the binding energy of the M_0^X exciton relative to the "free" exciton E_{gx}^X . E_b varies from 6 to 13 meV over the M_0^X line in various alloys. The abrupt cutoff of the M_0^X line shape at high-energy side is explained by the rapid decrease of $\langle W_{nr} \rangle$ as E_b decreases towards zero.

When the temperature is raised, the excitons make phonon-assisted "uphill" transitions to other states which have much shorter lifetimes (or larger values of W_{nr}) because they have small values of α . These higher states might be excited states of a given M_0^X exciton or another nearby higher-energy M_0^X localized state. The data on the temperature-dependent shift suggest that for the uphill "transition" the excitons with the smallest values of E_b will undergo the fastest thermal quenching, thus moving the short-wavelength cutoff of M_0^X towards greater values of E_b . It is also noted in Fig. 3 that the FWHM of the M_0^X band gets slightly narrower at higher temperatures. Accounting for the gain factors for the traces, the M_0^X is being "peeled off" of the high-energy portion of its line shape at higher temperatures. If M_0^X were due to excitons bound to impurity centers, the temperature rise would have thermally broadened its "inhomogeneous" linewidth. Neither can the factor of 4 intensity decrease from 2.6 to 4.9 K be found in or explained by any impurity-bound exciton system.

Figure 4 shows the temperature dependence of the M_0^X peak intensity. Over a limited temperature range from 2.5

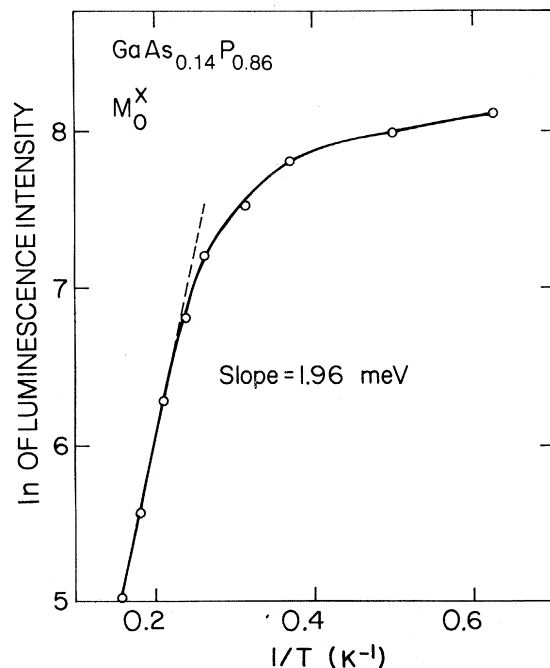


FIG. 4. A logarithmic plot of M_0^X peak intensity vs T^{-1} for $x=0.86$. The slope gives an activation energy of 1.96 meV.

to 6 K there is an activation energy of 2 meV. Since the distance from M_0^X to E_{gx}^X in this sample is 9.7 meV, such a low activation energy requires the existence of accessible states near by but higher in energy—either a 2-meV excited state of M_0^X or other nearby higher-energy M_0^X states. From the temperature data of Figs. 2 and 3, we conclude that such a 2-meV higher-energy state is nonradiative. This requires that the wave function of such a state will couple much more strongly with energy sinks such as D_0^X . This rapid variation of coupling as a function of exciton binding energy is verified from the fluorescence decay characteristics at different M_0^X energy positions (Fig. 10). The abrupt cutoff of the M_0^X line shape on its high-energy side is determined by such nonradiative coupling strength.

C. Saturation and Auger process

Another important characteristic of the M_0^X band is the relative saturation of its peak intensity with laser pump power. This is shown in Fig. 5 for the $x=0.86$ sample. With a laser image size of $50 \mu\text{m} \times 2 \text{mm}$ on the sample surface, D_0^X and M_0^X intensities increase linearly with pump power until the power reaches $8 \mu\text{W}$ (corresponding to an intensity of 8 mW/cm^2). Whereas D_0^X still increases linearly with power beyond this level, M_0^X begins to show a sublinear power dependence. At $600 \mu\text{W}$, M_0^X appears only as a small hump and it becomes unnoticeable beyond 20 mW . Such a small hump is easy to overlook and is sometimes mistaken to be the E_{gx}^X peak. We believe that this is the main reason why the M_0^X structure has escaped prior attention even though GaAsP alloys have been so extensively studied. The low power at which saturation occurs suggests that the M_0^X centers exist in a low concentration or have a fairly long lifetime. The slope in the intensity versus pump power curve changes from unity in

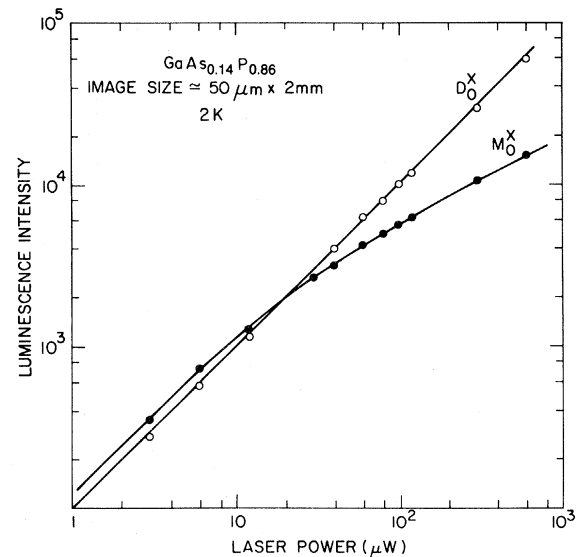


FIG. 5. Peak intensities of M_0^X and D_0^X vs 4880-Å laser power for the $x=0.86$ sample. The slope at the high-power end of the M_0^X curve is 0.51. Illuminated area of sample was $50 \mu\text{m} \times 2 \text{mm}$; thus a power of $1 \mu\text{W}$ is equivalent to a power density of $1 \mu\text{W/cm}^2$.

the linear regime to a value of 0.5 just as M_0^X becomes too weak relative to D_0^X to be observed. A similar saturation effect also occurs in the $x=0.5$ sample. The area of the laser image on the sample surface in this case was about 6 times larger than that for Fig. 5. The onset of saturation for the $x=0.5$ sample occurred at 33 mW/cm² compared to 8 mW/cm² for the $x=0.86$ sample, suggesting that the exciton lifetime of the $x=0.86$ sample is longer so that it has a lower saturation threshold. This observation is confirmed by the time-dependent measurements to be discussed in the next section.

At higher pump rates there is a finite probability of two or more excitons at the same M_0^X center. They will have large wave-function overlap, and their individual electron and hole components will experience mutual Coulomb interactions. An Auger process which eliminates excitons in pairs might then become favorable. At steady state the rate equation for the probability p of one exciton at a given M_0^X site (probability p^2 of two excitons) gives a result of the form

$$g = [p(W_0 + W_1 + W_{nr}) + p^2 W_A] n_s, \quad (3a)$$

where g is the generation rate, n_s is the number density of M_0^X sites, and W_A is the Auger decay rate. In the linear regime the number of excitons $n = pn_s$ obeys

$$n = g(W_0 + W_1 + W_{nr})^{-1} \quad (3b)$$

while at saturation

$$n = (gn_s/W_A)^{1/2}. \quad (3c)$$

Thus we expect a change in slope in a plot of $\ln I$ (or $\ln n$) vs $\ln P$ (or $\ln g$) from 1 to 0.5 with increasing laser power P .

D. Decay of luminescence following pulsed excitation

Figure 6 shows experimental data for three values of x on the decay of the peak of the luminescence spectrum following shutoff of the laser light. This occurred at 10.24 μ s. Counting intervals for each data point were 5.12 μ s for the lower two curves and 10.24 μ s for the upper curve. The curves are nonexponential. The solid straight line corresponds to exponentials with lifetimes of 49, 27, and 15 μ s for $x=0.86$, 0.66, and 0.50, respectively, but the curves do not extend over a sufficiently large time interval to establish that they are true radiative lifetimes. We shall refer to them as "characteristic decay times."

Figure 7 shows the laser-power-dependent decay curves $x=0.86$. There is a rapid initial nonexponential decay that is increased by raising the laser power. This increase is over an order of magnitude as the pump power is raised into the regime of saturation. This behavior is consistent with the Auger process mentioned in Sec. III C.

Figure 8 shows the rapid decrease of the characteristic decay times for the $x=0.86$ sample with increasing temperature. Since the intensity of M_0^X shows a rapid decrease in this temperature range (Fig. 3), we attribute the rise in the decay rate shown in Fig. 8 to the decrease in the nonradiative lifetime due to phonon-assisted transitions to more extended, short-lived localized states or uphill tunneling to other M_0^X centers followed by downhill tunneling to "sinks" such as D_0^X .

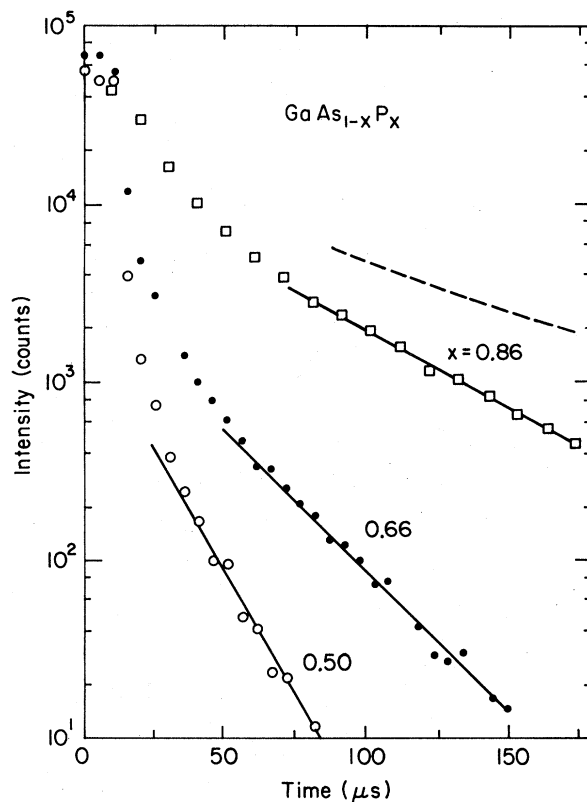


FIG. 6. Time dependence of M_0^X peak intensity following shutoff of the exciting laser light. Relative vertical scale for the three values of x is arbitrary.

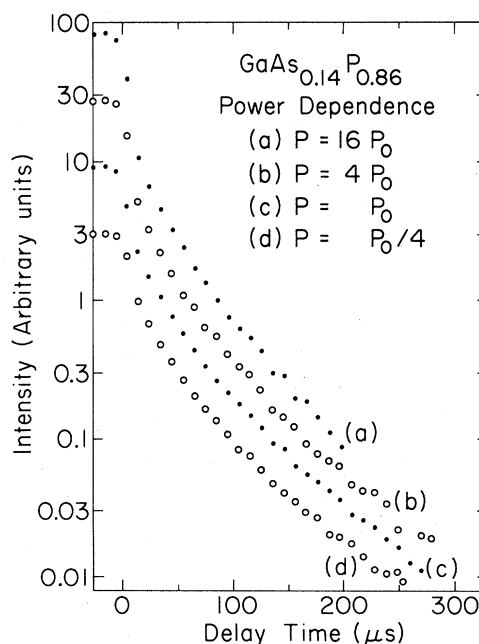


FIG. 7. Power-dependent decay curves for $x=0.86$ following laser shutoff at zero delay time. A power of P_0 corresponds to the onset of saturation. The curves have been arbitrarily shifted vertically for ease of viewing.

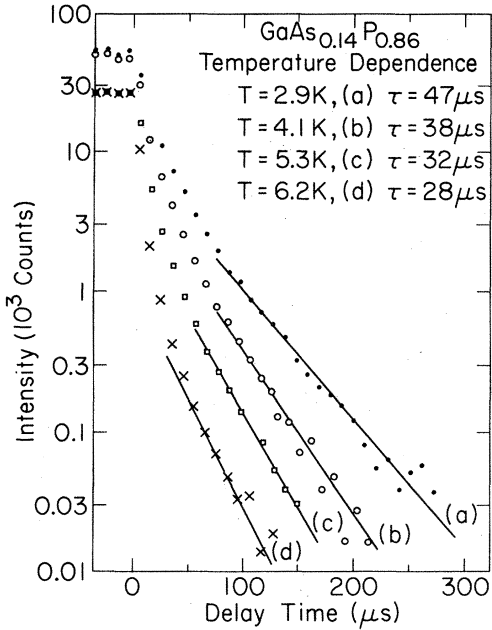


FIG. 8. Temperature-dependent decay curves for $x = 0.86$. Characteristic decay times at temperatures T are indicated. Curves have been shifted vertically.

Figure 9 shows how the M_0^X peak and its TA^X and LA^X sidebands depend on delay time for the $x = 0.65$ sample. The shift of the peaks to longer wavelengths with increasing delay t implies that the longer-lived centers have a deeper binding energy. This is consistent with the nonradiative tunneling decay model. Note that with increasing t the phonon sidebands increase relative to the no-phonon band. This is due to the distribution of no-phonon decay rates W_0 .¹² The one-phonon decay rate W_1 , being from a momentum conserving process, is expected to be unaffected by small difference in binding energy.

This variation of the intensity ratio of the no-phonon to its phonon sideband can be qualitatively understood as

$$-\dot{N}_0 = \frac{W_0 g (1 - e^{-(W_0 + W_1 + W_{nr})T}) e^{-(W_0 + W_1 + W_{nr})t}}{W_0 + W_1 + W_{nr}} = g [F_0(t) - F_0(t+T)], \quad (5a)$$

$$F_0(t) \equiv \frac{W_0 e^{-(W_0 + W_1 + W_{nr})t}}{W_0 + W_1 + W_{nr}} = W_0 \int_t^\infty e^{-(W_0 + W_1 + W_{nr})t'} dt'. \quad (5b)$$

Similarly the one-phonon radiative decay rate obeys

$$-\dot{N}_1(t) = g [F_1(t) - F_1(t+T)], \quad (6a)$$

where

$$F_1(t) \equiv W_1 \int_t^\infty e^{-(W_0 + W_1 + W_{nr})t'} dt'. \quad (6b)$$

The average of the distribution of radiative decays obey¹²

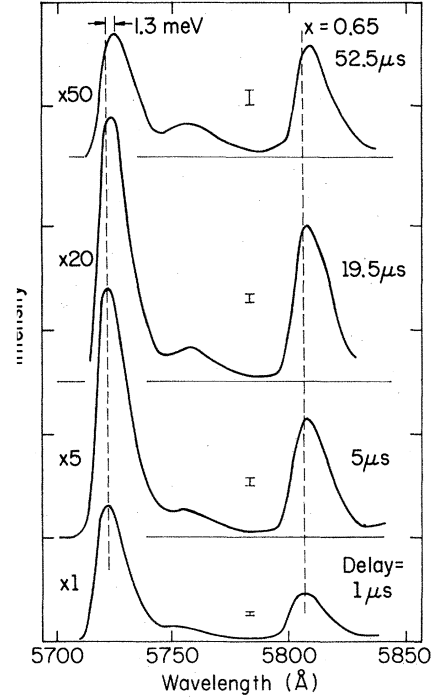


FIG. 9. M_0^X and its phonon sidebands at 2 K for $x = 0.65$ at various delay times. The laser was on for $10 \mu s$ for all curves. The counting gate width was $1 \mu s$ for the two lowest curves, $4 \mu s$ for the second curve from the top, and $10 \mu s$ for the top curve. Intensity scales have been adjusted for the difference in integration time.

follows: If the laser generates M_0^X centers at a rate g and is on for a time T , the number of M_0^X centers will be

$$N = \frac{g(1 - e^{-(W_0 + W_1 + W_{nr})T})}{W_0 + W_1 + W_{nr}}. \quad (4)$$

The no-phonon radiative decay rate is given by

$$\langle e^{-W_0 t'} \rangle = \frac{1}{1 + \langle W_0 \rangle t'}, \quad (7a)$$

$$\langle W_0 e^{-W_0 t'} \rangle = \frac{\langle W_0 \rangle}{(1 + \langle W_0 \rangle t')^2}. \quad (7b)$$

For the average over the nonradiative decays, we introduce a function $Q(t)$:

$$\langle e^{-W_{nr}(t)} \rangle = Q(t). \quad (7c)$$

Equations 5(a) and 5(b) and 7(b) and 7(c) yield

$$-\langle \dot{N}_0(t) \rangle = g \langle W_0 \rangle \int_t^{t+T} \frac{Q(t') e^{-W_1 t'}}{(1 + \langle W_0 \rangle t')^2} dt', \quad (8a)$$

and Eqs. 6(a) and 6(b) and 7(a) and 7(c) yield

$$-\langle \dot{N}_1(t) \rangle = gW_1 \int_t^{t+T} \frac{Q(t')e^{-W_1 t'} dt'}{(1 + \langle W_0 \rangle t')} \quad (8b)$$

For a time $t_1 \ll \langle W_0 \rangle^{-1}$ we obtain

$$\frac{\langle \dot{N}_1(t_1) \rangle}{\langle \dot{N}_0(t_1) \rangle} = \frac{W_1}{\langle W_0 \rangle}, \quad (9a)$$

and for a time $t_2 \gg T$ we obtain

$$\frac{\langle \dot{N}_1(t_2) \rangle}{\langle \dot{N}_0(t_2) \rangle} = \frac{W_1}{\langle W_0 \rangle} (1 + \langle W_0 \rangle t_2). \quad (9b)$$

By applying Eqs. 9(a) and 9(b) to the data in Fig. 9 with $t_1 = 1$, $t_2 = 52.5 \mu\text{s}$, we find

$$\langle W_0 \rangle \approx \frac{1}{35}, \quad (10a)$$

$$W_1 \approx \frac{1}{100} \quad (10b)$$

(measured in units of inverse μs). These are rough estimates. More time-dependent data are required for a detailed analysis.

The shift in M_0^X position to larger binding energies with increasing time delay apparent from Fig. 9 implies different time dependences for different portions of the M_0^X line. This is seen more clearly in Fig. 10. The more weakly bound portion of the M_0^X line (c) decays much more rapidly than either the center of the line (b) or the more strongly bound portion of the line (a).

E. Relative intensities

The three spectra shown in Fig. 1 were measured under identical conditions in a same run. If we assume that both the concentration and the distribution of nonradiative lifetimes of M_0^X centers are independent of x , then the intensities of the M_0^X line should be proportional to the mean radiative decay rate $\langle W_0 \rangle$, which in turn should be proportional to the mean-square random alloy potential $\delta v^2 = x(1-x)(dE_g/dx)^2$ divided by Δ^2 , where Δ is the difference between the M_0^X energy and that of the direct gap at the Γ point.^{11,12} Values for the measured relative intensity, δv , Δ , and $\delta v^2/\Delta^2$ are given in Table II. It is seen that the relative intensity of M_0^X approximately obeys the expected proportionality of $\delta v^2/\Delta^2$. The LA sideband has the same recombination channel as the zero-phonon line, but an electron-phonon matrix element replaces δv , hence W_1 and the LA_M^X intensity should be proportional to Δ^{-2} , which is approximately the case. The other phonon sidebands decay through higher direct gaps and hence will have smaller effective values of Δ^{-2} . (The data for

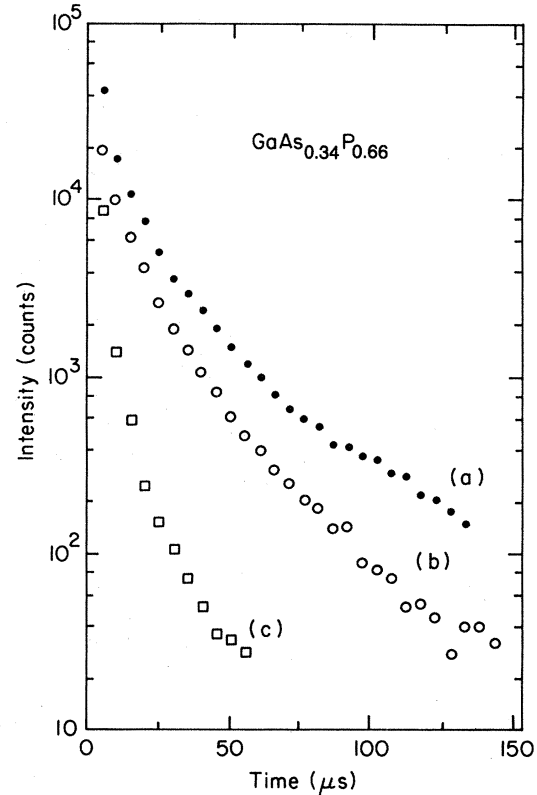


FIG. 10. Time decays for three portions of the M_0^X line for $x = 0.66$. Open circles (b) refer to the peak of the line (at short-time delays); closed circles (a) refer to that portion of the line with 2.45 meV greater binding energy than the peak; squares (c) refer to that portion of the line with 2.45-meV less binding energy than the peak.

the TA sideband are obtained from the time-delayed spectra shown in Fig. 2 of Ref. 10.)

F. Nonradiative decay

We believe that the principal reason for the differences among the three curves in Fig. 6 is the dependence upon x of $\langle W_0 \rangle$ and W_1 as discussed in Sec. III E. The decay of the $x = 0.50$ curve is primarily radiative, that of the $x = 0.86$ curve is primarily nonradiative; the dashed line is our estimate for the nonradiative part $Q(t)$. This estimate was made by correcting the experimental curve for the radiative dependence [Eq. 8(a)] using

$$\langle W_0 \rangle = 0.40, \quad (11a)$$

$$W_1 = 0.26. \quad (11b)$$

TABLE II. Relative intensities of M_0^X and its phonon satellites; δv is the rms random potential and Δ is the energy difference from M_0^X to the direct gap.

X	M_0^X	TA_M^X	LA_M^X	TO_M^X	δv (meV)	Δ (meV)	$(\delta v/\Delta)^2$
0.86	2.7	0.49	1.54	0.42	176	398	0.20
0.66	8.2	0.77	3.8	0.51	208	213	0.95
0.50	80.0	4.0	33.6	2.4	175	63	7.72

(measured in units of inverse $100 \mu\text{s}$).

The calculation of $Q(t)$ has been given in integral form by Thomas *et al.*¹⁹ and a useful approximation by Searle *et al.*²⁰ Because of the small range of delay times used so far and the difficulty of accurately correcting for radiative decays, we do not yet have sufficiently good data on $Q(t)$ to compare with these results.

IV. SUMMARY AND CONCLUSIONS

The strong reduction in intensity of M_0^X with increasing temperature shown in Figs. 2, 4, and 8 is evidence of accessibility to a given M_0^X center of a shorter-lived, higher-energy state—either an excited state of the original center or a neighboring higher-energy M_0^X center. The power dependence presented in Figs. 5 and 7 is evidence that the radiative decay processes of M_0^X can be saturated before the nonradiative decay processes. This is unlike the case of indirect $\text{GaAl}_x\text{As}_{1-x}$ near crossover to direct behavior,¹¹ where the radiative decays are much more rapid, and where the nonradiative processes saturate first. Saturation in $\text{GaAs}_{1-x}\text{P}_x$ is attributed to Auger decays of biexcitons.

Figure 9 and 10 clearly show that the more weakly bound portion of the M_0^X centers decay more rapidly by an

order of magnitude over the M_0^X line shape, consistent with a tunneling picture of nonradiative decays. In addition, Fig. 9 shows that there is a distribution of zero-phonon radiative decay rates W_0 and that $\langle W_0 \rangle \sim (35 \mu\text{s})^{-1}$.

While none of these properties of M_0^X centers prove that they are due to excitons bound to fluctuations in the alloy potential, all are consistent with such a picture. The X -point phonon sidebands point to M_0^X as an effective-mass center, not an extrinsic center of the isoelectronic type. In a planned future paper we shall develop further the model for the density of states of M_0^X centers sketched in Ref. 10 and present model calculations for the time-dependent decays.

ACKNOWLEDGMENTS

We thank D. J. Wolford and B. G. Streetman for their samples and J. P. Wolfe for use of equipment for time-resolved spectra. This work was supported by the National Science Foundation under Grant Nos. DMR-79-02780 and DMR-82-03523 with institutional support through the Materials Research Laboratories Program Grant No. DMR-80-20250. All data were taken at the University of Illinois.

¹A. N. Pikhtin, *Fiz. Tekh. Poluprovodn.* **11**, 425 (1977) [*Sov. Phys.—Semicond.* **11**, 245 (1977)].

²S. Sakai and T. Sugano, *J. Appl. Phys.* **50**, 4143 (1979).

³Zh. I. Alferov, E. L. Portnoi, and A. A. Rogachev, *Fiz. Tekh. Poluprovodn.* **2**, 1194 (1968) [*Sov. Phys.—Semicond.* **2**, 1001 (1969)].

⁴S. D. Baranovski and A. L. Efros, *Fiz. Tekh. Poluprovodn.* **12**, 2233 (1978) [*Sov. Phys.—Semicond.* **12**, 1328 (1978)].

⁵L. G. Suslina, A. K. Plyukhin, D. L. Fedorov, and A. G. Areshkin, *Fiz. Tekh. Poluprovodn.* **12**, 2238 (1978) [*Sov. Phys.—Semicond.* **12**, 1331 (1978)].

⁶A. N. Pikhtin, V. N. Razbegaev, and D. A. Yas'kov, *Fiz. Tekh. Poluprovodn.* **7**, 471 (1973) [*Sov. Phys.—Semicond.* **7**, 337 (1973)].

⁷A. L. Efros, *Usp. Fiz. Nauk.* **111**, 451 (1973) [*Sov. Phys.—Usp.* **16**, 789 (1974)].

⁸P. W. Anderson, *Phys. Rev.* **109**, 1492 (1958).

⁹N. F. Mott and E. A. Davis, *Electronic Processes in Non-Crystalline Materials* (Oxford University Press, London, 1979).

¹⁰Shui Lai and M. V. Klein, *Phys. Rev. Lett.* **44**, 1087 (1980).

¹¹M. D. Sturge, E. Cohen, and R. A. Logan, *Phys. Rev. B* **27**, 2362 (1983).

¹²M. V. Klein, M. D. Sturge, and E. Cohen, *Phys. Rev. B* **25**, 433 (1982).

¹³D. J. Wolford, B. G. Streetman, Shui Lai, and M. V. Klein, *Solid State Commun.* **32**, 51 (1979).

¹⁴J. L. Yarnell, J. L. Warren, R. G. Wenzel, and P. J. Dean, in U. S. Atomic Energy Commission Report No. LA-DC-9228, 1968 (unpublished).

¹⁵H. Mathieu, P. Merle, and E. L. Ameziane, *Phys. Rev. B* **15**, 2048 (1977).

¹⁶J. L. T. Waugh and G. Dolling, *Phys. Rev.* **132**, 2410 (1963).

¹⁷L. Genzel and W. Bauhofer, *Z. Phys. B* **25**, 13 (1976).

¹⁸A. Baldareschi, *J. Lumin.* **7**, 79 (1973).

¹⁹D. G. Thomas, J. J. Hopfield, and W. M. Augustiniak, *Phys. Rev.* **140**, A202 (1965), Eq. (13).

²⁰T. M. Searle, T. S. Nashashibi, I. G. Austin, R. Devonshire, and G. Lockwood, *Philos. Mag. B* **39**, 389 (1979), Eqs. 4(a) and 4(b).